HHS Public Access

Author manuscript

Nat Immunol. Author manuscript; available in PMC 2013 November 01.

Published in final edited form as:

Nat Immunol. 2013 May ; 14(5): 480–488. doi:10.1038/ni.2563.

Receptor interacting protein kinase 2-mediated mitophagy regulates inflammasome activation during virus infection

Christopher Lupfer[1], **Paul G. Thomas**[1], **Paras K. Anand**[1], **Peter Vogel**[3], **Sandra Milasta**[1], **Jennifer Martinez**[1], **Gonghua Huang**[1], **Maggie Green**[1], **Mondira Kundu**[2], **Hongbo Chi**[1], **Ramnik J. Xavier**[4,5,6], **Douglas R. Green**[1], **Mohamed Lamkanfi**[7,8], **Charles A. Dinarello**[9], **Peter C. Doherty**[1,10], and **Thirumala-Devi Kanneganti**[1]

[1]Department of Immunology, St. Jude Children's Research Hospital, Memphis, TN 38105, United States

[2]Department of Pathology, St. Jude Children's Research Hospital, Memphis, TN 38105, United States

[3]Veterinary Pathology Core, St. Jude Children's Research Hospital, Memphis, TN 38105, United States

[4]Gastrointestinal Unit and Center for the Study of Inflammatory Bowel Disease, Harvard Medical School, Boston, Massachusetts 02114, United States

[5]Center for Computational and Integrative Biology, Massachusetts General Hospital, Harvard Medical School, Boston, Massachusetts 02114, United States

[6]The Broad Institute of MIT and Harvard, 7 Cambridge Center, Cambridge, Massachusetts 02142, United States

[7]Department of Biochemistry, Ghent University, VIB, B-9000 Ghent, Belgium

[8]Department of Medical Protein Research, VIB, B-9000 Ghent, Belgium

[9]Department of Medicine, University of Colorado Denver, Aurora, CO 80045, United States

[10]Department of Microbiology and Immunology, University of Melbourne, Vic 3010, Australia

Correspondence should be addressed to: Thirumala-Devi Kanneganti Department of Immunology, MS #351 St Jude Children's Research Hospital 262 Danny Thomas Place Memphis TN 38105-2794, USA Tel: (901) 595-3634; FAX: (901) 595-5766 Thirumala-Devi.Kanneganti@stjude.org.

Author contributions C.L. designed and conducted experiments and wrote the manuscript. P.G.T. helped conduct the initial experiments *in vivo* in *Ripk2*$^{-/-}$ mice and helped design T cell experiments. P.K.A. conducted experiments with *Listeria monocytogenes* and helped write the manuscript. P.V. helped design experiments and interpret histopathology data. S.M. helped design and conduct experiments related to mitophagy and mitochondrial damage. J.M. helped design experiments related to mitophagy and mitochondrial damage. G.H. helped design and conduct experiments with p38 conditional KO mice. M.G. conducted experiments for IL-18 and NF-κB and MAPK signaling. M.K. helped design experiments and provided *Ulk1*$^{-/-}$ mice and other reagents for ULK1 experiments. H.C. helped design experiments and provided p38 conditional KO mice. R.J.X. helped design experiments and provided reagents for ATG16 related experiments and autophagy in general. D.R.G. helped design experiments and provided reagents, *Ulk1*$^{-/-}$ mice, and ATG7 conditional KO mice for mitophagy related experiments. M.L. helped design experiments and provided reagents for caspase-1 activation and interaction studies. C.A.D. helped design experiments and provided reagents for IL-18 neutralization studies. P.C.D. helped design experiments and provided reagents for T cell experiments. T-D.K. conceived project, designed experiments, helped write the manuscript, and managed collaborations and funding.

Abstract

NOD2 receptor and the cytosolic protein kinase RIPK2 regulate NF-κB and MAP kinase signaling during bacterial infections, but the role of this immune axis during viral infections has not been addressed. We demonstrate that *Nod2*$^{-/-}$ and *Ripk2*$^{-/-}$ mice are hypersusceptible to influenza A virus infection. *Ripk2*$^{-/-}$ cells displayed defective mitophagy leading to enhanced mitochondrial superoxide production and accumulation of damaged mitochondria resulting in increased NLRP3 inflammasome activation and IL-18 production. RIPK2 regulated mitophagy in a kinase-dependent manner by phosphorylating the mitophagy inducer ULK1. Accordingly, *Ulk1*$^{-/-}$ cells displayed enhanced mitochondrial superoxide production and caspase-1 activation. These results demonstrate a role for NOD2-RIPK2 signaling in protection against virally triggered immunopathology by negatively regulating NLRP3 inflammasome activation and IL-18 production via ULK1-dependent mitophagy.

Keywords

RIPK2; NLR; Caspase-1; inflammasome; Influenza; IL-18; autophagy; mitophagy

Seasonal influenza A virus (IAV) epidemics are a major cause of morbidity and economic loss, with annual mortality rates estimated in the 9,000–45,000 range for the USA alone[1]. In addition, global pandemics of antigenically-novel IAV strains that emerge from avian and domestic swine reservoirs can result in the death of millions. The catastrophic 1918 H1N1 pandemic was characterized by an unusually high incidence of rapid lethality in otherwise healthy young adults[2]. More recently, similar pathological profiles have been documented for infections caused by the highly virulent avian H5N1 IAV strains[3, 4]. In both humans and animal models, infections with these highly-pathogenic strains were characterized by rapid onset of a pro-inflammatory `cytokine storm' that caused damage to the lung epithelium, edema, and hemorrhage. Relative to the host responses induced by low-pathogenicity influenza viruses, infections with the 1918 H1N1 or highly-pathogenic H5N1 viruses are associated with markedly increased neutrophil and macrophage infiltration and elevated cytokines and chemokines, including IL-1β, IFN-γ and TNF[4–6]. Thus, in addition to virus replication, it has become increasingly clear that the severity of the inflammatory response to IAV infection contributes significantly to morbidity and mortality.

The signaling pathways regulating the innate immune response to IAV infection are now being defined, with obvious roles for the endocytic Toll-like receptors TLR3[7] and TLR7[8], and the cytosolic receptor RIG-I[9]. Recently, members of the Nod-like receptor (NLR) family have also been shown to recognize IAV in the cytosolic compartment[10–12]. NLRP3 detects IAV infection through multiple mechanisms, including ion flux generated by the virus encoded M2 ion channel[11] and via the recognition of viral RNA[10, 13]. These signals serve to activate the inflammasome, a macromolecular complex consisting of caspase-1, the adaptor protein ASC and NLRP3[14]. Inflammasome activation leads to the cleavage of numerous substrates, including pro-IL-1β and pro-IL-18, and the initiation of the pro-inflammatory form of cell death known as pyroptosis[15].

Autophagy is a cellular process where cytoplasmic double membrane vesicles are formed and engulf cytoplasmic contents. Several forms of autophagy exist, including macroautophagy, where long-lived proteins or organelles are engulfed and degraded for recycling[16]. It should be noted that macroautophagy was recently shown to be a critical modulator of inflammasome activation[17], but it is unknown if this is applicable during viral infection. Another subset of the autophagic process is known as mitophagy, wherein mitochondria are specifically degraded in response to damage or developmental cues[18, 19]. Finally, xenophagy is an innate immune mechanism where invading cytosolic pathogens are captured and degraded to prevent their further spread and for antigen presentation to initiate adaptive immunity[20, 21].

Receptor interacting protein kinase 2 (RIPK2 also known as RIP2 or RICK) is a critical mediator of inflammatory responses to bacterial infections, where it is activated by the NLRs NOD1 and NOD2. RIPK2 is involved in the induction of xenophagy in response to bacterial infections[20, 22, 23]. Furthermore, the sensing of bacterial peptidoglycan components activates the NOD1-NOD2-RIPK2 axis and signals through NF-κB and MAP kinase (MAPK) to activate inflammatory cells and to promote secretion of proinflammatory cytokines and chemokines[24]. Although NOD2 regulates type I interferon production during viral infections independently of RIPK2[25, 26], the putative roles of RIPK2 during IAV infection have not been determined. Here, we demonstrate that *Ripk2*$^{-/-}$ mice are hypersusceptible to IAV infection. RIPK2 dampens inflammasome activation and IL-18 secretion, which contribute critically to disease progression. Mechanistically, increases in IL-18 production and inflammasome activation are a consequence of defective mitophagy induction in IAV-infected *Ripk2*$^{-/-}$ mice and immune cells. Finally we demonstrate that activation of the critical autophagy inducer ULK1 is reduced in *Ripk2*$^{-/-}$ cells and that *Ulk1*$^{-/-}$ cells also display increased inflammasome activation and reduced mitophagy. Our results highlight a previously unknown RIPK2-dependent signaling network that negatively regulates inflammasome activation through mitophagy during viral infection.

Results

RIPK2 protects against severe IAV infection

To examine the potential role of NOD2 and RIPK2 in the immune response to IAV infection, wildtype (WT), *Nod2*$^{-/-}$ and *Ripk2*$^{-/-}$ mice were challenged intranasally (i.n.) with the virulent influenza A/PR/8/34 (PR8) H1N1 virus and survival was monitored over time. Relative to wildtype (WT) controls, *Nod2*$^{-/-}$ and *Ripk2*$^{-/-}$ mice were significantly more susceptible (Fig. 1a). While signs of pathological damage to the lungs of WT mice were minimal by day (d) 2 after PR8 inoculation, lung sections of both knockout mouse lines showed marked pathological changes characterized by greater pulmonary airway obstruction and increased cell death on d2 and d7 after infection (Fig. 1b–d **and data not shown**). Moreover, airway obstruction of IAV-infected *Ripk2*$^{-/-}$ mice consisted mainly of neutrophils (Fig. 1e). While neutrophil counts were elevated in the *Ripk2*$^{-/-}$ whole lung on d2 and d7, no increases were observed in the numbers of other myeloid cells (Fig. 1f–g). Despite the increased susceptibility of *Ripk2*$^{-/-}$ mice to IAV infection, lung virus titers were

comparable to those in the WT controls (Fig. 1h). Thus, NOD2 and RIPK2 protects against severe IAV infection, although this is not correlated with the extent of virus replication.

RIPK2 regulates IFN-γ and IL-18

Given that the inflammatory response to IAV is thought to contribute to mortality[3, 4], we investigated the role of RIPK2 in cytokine production. To this end, whole lung homogenates were taken on days 2 and 7 after i.n. challenge of WT and *Ripk2*$^{-/-}$ mice with the PR8 virus, and the extent of inflammatory mediator production was determined by ELISA. Although RIPK2 regulates IL-6 and TNF production during bacterial infections[27], no significant differences in the levels of these cytokines were observed in lungs of virus-infected WT and *Ripk2*$^{-/-}$ mice (Fig. 2a). In contrast, IFN-γ, a known mediator of inflammation in viral immunity[28], and IL-18 were significantly upregulated in *Ripk2*$^{-/-}$ mice (Fig. 2b). IL-18 was originally identified as an IFN-γ-inducing cytokine[29], suggesting that IFN-γ production might be consequential to increased IL-18 release in IAV-infected *Ripk2*$^{-/-}$ mice. Previous studies have shown the chemokines CCL2 (MCP-1) and CXCL10 (IP-10) were induced by IL-18 and IFN-γ[30] and accordingly, we observed elevated production of both CCL2 and CXCL10 in IAV-infected *Ripk2*$^{-/-}$ mice (Fig. 2c). These results indicate that increased susceptibility to IAV infection in *Ripk2*$^{-/-}$ mice is associated with exacerbated production of IL-18 and IFN-γ.

IL-18 antagonism in *Ripk2*$^{-/-}$ mice improves survival

We hypothesized that increased IL-18 production was responsible for the elevated IAV susceptibility of *Ripk2*$^{-/-}$ mice. To test this, *Ripk2*$^{-/-}$ mice were injected intraperitoneally (i.p.) with anti-IL-18 neutralizing antibody 3h prior to PR8 infection. This treatment significantly reduced IL-18 and IFN-γ levels in the lungs of IAV-infected *Ripk2*$^{-/-}$ mice (Fig. 3a). This was followed by significantly reduced CCL2 levels, while the concentration of the chemokines CXCL10, CXCL1 (KC) and CCL3 (MIP-1α) protein- albeit not statistically significant - showed a trend towards diminished expression (Supplementary Fig. 1a). Furthermore, IL-18 neutralization dampened virus-induced lung pathology and airway neutrophilia (Fig. 3b–c and Supplementary Fig. 1b), and significantly improved survival (Fig. 3d). These results suggest that increased IL-18 production drives elevated morbidity and mortality in IAV-infected *Ripk2*$^{-/-}$ mice. To further confirm the critical role of IL-18 in this process, we generated mice lacking both RIPK2 and IL-18 (*Ripk2*$^{-/-}$*Il18*$^{-/-}$ mice) and challenged these animals with a lethal dose of IAV. As with *Ripk2*$^{-/-}$ mice receiving IL-18-neutralizing antibodies, genetic ablation of IL-18 rescued the hypersensitive response of *Ripk2*$^{-/-}$ mice; tissue neutrophil infiltration and mortality rates returned to levels comparable to those of infected WT mice (Fig. 3e–f). Overall, these results demonstrate a critical role for elevated IL-18 production increasing morbidity and mortality in IAV-infected *Ripk2*$^{-/-}$ mice.

Immune and lung cells contribute to elevated IL-18

We next set out to identify the cellular compartments that contribute to RIPK2-mediated modulation of IL-18. Bone marrow (BM) chimeras were generated that selectively expressed RIPK2 in the radiation-sensitive (donor BM) or radiation-resistant (recipient lung)

compartments. These chimeric mice were subsequently infected i.n. with PR8, and IL-18 production was assessed by immunohistochemistry (IHC) and ELISA. Both *Ripk2*$^{-/-}$ hematopoietic and non-immune (likely lung epithelial) cells contributed to increased production of IL-18 in the pulmonary tract of IAV-infected *Ripk2*$^{-/-}$ mice (Fig. 4a–b, and Supplementary Fig. 2a).

Innate and adaptive lymphocytes are hyperactivated

We next examined the cellular populations that were responsible for the increased IFN-γ observed in *Ripk2*$^{-/-}$ mice. Both NK cells and CD8^{+} T cells isolated from PR8-infected *Ripk2*$^{-/-}$ mice produced larger quantities of IFN-γ on a per-cell basis and were more highly activated, although the absolute numbers of these cells remained similar to those in WT mice (Fig. 4c–f, and Supplementary Fig. 2b–d). These results indicate that increased IL-18 in *Ripk2*$^{-/-}$ mice subsequently leads to increased IFN-γ production from innate and adaptive cell populations.

NOD2-RIPK2 axis regulates caspase-1 activation and IL-18

NOD2 was reported to regulate type I IFN during IAV infection[25, 26]. We therefore examined type I IFN levels in IAV-infected *Ripk2*$^{-/-}$ mice. Although we confirmed the reported defect in type I IFN production in *Nod2*$^{-/-}$ alveolar macrophages, *Ripk2*$^{-/-}$ macrophages produced type I IFN (IFN-β) protein in amounts similar to those of WT cells (data not shown), suggesting that differences in type I IFN signaling are unlikely to account for the observed hypersensitive phenotype of *Ripk2*$^{-/-}$ mice. Similarly, we found no significant differences in activation of NF-κB (pIκBα) and MAPK (pERK) pathways in IAV-infected *Ripk2*$^{-/-}$ bone marrow derived dendritic cells (BMDCs) (data not shown). We therefore analyzed processes directly regulating IL-18 maturation rather than IL-18 transcript abundance. Unlike most cytokines, IL-1β and IL-18 are produced as propeptides that require proteolytic maturation by the cysteine protease caspase-1 in order to be released in their biologically active forms[31]. Notably, both caspase-1 activation and release of mature IL-18 and IL-1β were markedly increased in PR8 infected *Ripk2*$^{-/-}$ and *Nod2*$^{-/-}$ BMDCs (Fig. 5a–b). Although we initially detected increased IL-18 levels *in vivo*, low amounts of IL-1β likely confounded detection of differences in this cytokine *in vivo* (Supplementary Fig. 3a). Next, we examined caspase-1 activation to other IAV infections. We observed that the ×31 low pathogenicity virus also elicited higher caspase-1 activation in *Ripk2*$^{-/-}$ BMDCs (Supplementary Fig. 3b). We also examined inflammasome activation during infection with bacteria known to activate the RIPK2 signaling pathway. Infection with *Listeria* failed to augment caspase-1 processing and IL-18 production in *Ripk2*$^{-/-}$ and *Nod2*$^{-/-}$ BMDCs (Figs. 5c–d). This enhancement of inflammasome activation by IAV in *Ripk2*$^{-/-}$ BMDCs was dependent on NLRP3, as the NLRP3 specific inhibitor glyburide[32] significantly inhibited caspase-1 activation and IL-18 production (Fig. 5e–f). In the case of *Listeria* infection, the AIM2 inflammasome plays a predominant role in inflammasome activation[33]. In agreement, *Aim2*$^{-/-}$ BMDCs showed nearly complete impairment in caspase-1 activation following *Listeria* infection (Fig. 5g). These data indicate that enhanced NLRP3 inflammasome activation occurs in *Ripk2*$^{-/-}$ BMDCs during IAV infection, but not *Listeria* infection, indicating that this pathway is not a global disregulation of inflammasome activation, but specific to the NLRP3 inflammasome.

RIPK2 regulates the NLRP3 inflammasome through autophagy

To determine the mechanism by which RIPK2 dampens inflammasome activation, we first assessed the effect of RIPK2 overexpression on caspase-1 maturation and IL-18 release in transfected 293T cells. In agreement with published reports[34], overexpressed RIPK2 interacted with caspase-1 but this interaction enhanced, rather than inhibited, caspase-1 processing and IL-18 release (data not shown) indicating that RIPK2 overexpression is not capable of directly inhibiting inflammasome activation. Because *Ripk2*$^{-/-}$ BMDCs do not display a global defect in inflammasome activation (see Fig. 5), this suggests that RIPK2 may modulate caspase-1 indirectly in our model. In this regard, autophagy was recently described to negatively regulate inflammasome activation during bacterial infections[17, 35, 36]. We therefore hypothesized that *Ripk2*$^{-/-}$ and *Nod2*$^{-/-}$ BMDCs might be defective in autophagy induction in response to IAV infection. LC3 lipidation is an important step in the formation of autophagosomes. Therefore, one method to examine autophagic activity is to examine the level of LC3-II (lipidated form). In agreement with our hypothesis, *Ripk2*$^{-/-}$ and *Nod2*$^{-/-}$ BMDCs had significantly lower amounts of LC3-II protein than WT BMDCs infected with either PR8 or ×31 (Fig. 6a and Supplementary Fig. 4a). It should be noted that turnover of autophagosomes, which results from their fusion with lysosomes, was not affected by IAV infection in WT or *Ripk2*$^{-/-}$ BMDCs as treatment with the lysosomal fusion inhibitor chloroquine resulted in the expected accumulation of LC3-II^{+} puncta by immunofluorescence and LC3-II conversion by Western blot (Figure 6b–c and Supplementary Fig. 4b). Finally, we counted autophagosomes by electron microscopy and determined that *Ripk2*$^{-/-}$ BMDCs had significantly fewer autophagosomes following IAV infection than WT BMDCs (Supplementary Fig. 4c–e). To establish the potential role of differential autophagy induction in caspase-1 activation, we compared WT, *Ripk2*$^{-/-}$ and LysM-Cre^{+}*Atg7*$^{flox/flox}$ bone marrow-derived macrophages (BMDMs) which lack a critical component of the autophagy machinery in myeloid cells. Both *Ripk2*$^{-/-}$*and Atg7*$^{-/-}$ BMDMs responded to IAV infection with enhanced caspase-1 activation relative to WT macrophages (Supplementary Fig. 4f). To further confirm the role of autophagy in *Ripk2*$^{-/-}$ cells, we treated *Ripk2*$^{-/-}$ BMDCs with rapamycin to force the induction of autophagy. Following rapamycin treatment, IL-18 production and caspase-1 activation in *Ripk2*$^{-/-}$ BMDCs was diminished to WT levels (Fig. 6d–e). We next verified the role of autophagy *in vivo* and found that LC3-II protein was reduced in the lungs of IAV infected *Ripk2*$^{-/-}$ mice as well (Fig. 6f). We also examined the effects of inducing autophagy *in vivo* with rapamycin treatment in IAV-infected *Ripk2*$^{-/-}$ mice and observed that rapamycin treatment dampened neutrophil recruitment and inflammatory cytokine production in *Ripk2*$^{-/-}$mice (Fig. 6g–h). Together, these results demonstrate that RIPK2 negatively regulates inflammasome activation, inflammatory cytokine production and neutrophil recruitment by inducing autophagy in IAV-infected cells and mice.

Viral RNA genomes activate autophagy through NOD2-RIPK2

To examine the mechanism by which NOD2 and RIPK2 induce mitophagy, we expressed RIPK2 and NOD2 in the presence or absence of IAV infection and determined that infection induces an interaction between RIPK2 and NOD2 (Supplementary Fig. 5a). Next, we determined the viral ligand that triggers NOD2-RIPK2 signaling. The cytosolic delivery of

viral RNA analogues (poly I:C + lyovec transfection) was capable of inducing LC3-II conversion in a RIPK2- and NOD2- dependent manner (Supplementary Fig. 5b). However, extracellular delivery of naked poly I:C induced LC3-II conversion independently of the RIPK2 pathway (Supplementary Fig. 5c). We also transfected BMDCs with purified viral RNA (vRNA) genomes and determined that IAV vRNA induces autophagy in a RIPK2 dependent manner (Supplementary Fig. 5d). Finally, transfection of IAV vRNA followed by ATP treatment resulted in enhanced IL-18 production in both *Ripk2*$^{-/-}$ and *Nod2*$^{-/-}$ BMDCs (Supplementary Fig. 5e). These data indicate that cytosolic viral genomes activate the cytosolic NOD2-RIPK2 signaling pathway to trigger autophagy.

NOD2-RIPK2 mediated mitophagy regulates the inflammasome

In addition to preserving cellular energy stores, autophagy is linked to the removal of damaged mitochondria. Notably, mitochondrial damage and the subsequent release of reactive oxygen species (ROS) is linked to activation of the NLRP3 inflammasome[34,37]. We thus hypothesized that defective mitophagy induction in IAV-infected RIPK2-deficient cells triggered increased inflammasome activation due to the accumulation of damaged mitochondria. To investigate this possibility, we examined mitochondrial superoxide (SOX) production following IAV infection. IAV infection increased mitochondrial SOX production in *Ripk2*$^{-/-}$ and *Nod2*$^{-/-}$ BMDCs to a markedly higher extent than in WT BMDCs (Fig. 7a and Supplementary Fig. 6a–b). To further confirm that mitochondrial damage was responsible for our observed phenotype we also examined mitochondrial SOX during *Listeria* infection. Although *Listeria* infection generated a more robust production of SOX compared to IAV, there was no difference between WT and *Ripk2*$^{-/-}$ cells (Fig. 7b and Supplementary Fig. 6c). We also counted damaged mitochondria (disrupted cristae) by electron microscopy and determined that IAV infected *Ripk2*$^{-/-}$ BMDC have a higher ratio of damaged to healthy mitochondria than WT controls (Supplementary Fig. 6d). We further confirmed the role of mitophagy in our model by staining BMDCs infected with IAV or *Listeria* with MitoTracker Green and examined the fluorescence intensity by flow cytometry. Cells with higher geometric mean fluorescence intensity (MFI) indicate an accumulation of mitochondria. Although *Ripk2*$^{-/-}$ cells tended to have more mitochondria even before infection, we observed that IAV infected *Ripk2*$^{-/-}$ BMDC but not WT had an increase in mitochondria, and furthermore, this increase was not seen with *Listeria* infected *Ripk2*$^{-/-}$ cells (Fig. 7c and Supplementary Fig. 7a–c). We also confirmed these findings by isolating DNA from BMDCs and comparing the ratio of nuclear DNA to mitochondrial DNA. Using this approach, we also determined that there are more mitochondria in IAV infected *Ripk2*$^{-/-}$ BMDCs compared to WT BMDCs (Supplementary Fig. 7d). As mitophagy appears to be defective in *Ripk2*$^{-/-}$ cells, resulting in greater production of mitochondrial SOX, we treated *Ripk2*$^{-/-}$ BMDCs with N-acetyl cysteine (NAC), a general ROS inhibitor, and found significantly reduced IL-18 levels and caspase-1 activation relative to control-treated *Ripk2*$^{-/-}$ BMDCs that were infected with IAV (Fig. 7d–e). Similar results were obtained with the specific mitochondrial SOX inhibitor mitoTEMPO (Fig. 7f). To confirm the specificity of these results, we also treated *Ripk2*$^{-/-}$*Listeria*-infected BMDCs with NAC. In agreement with the role for the AIM2 inflammasome in *Listeria* infection, we observed little or no effect of NAC treatment during *Listeria* infection (Supplementary Fig. 7e). Finally, we verified directly that mitophagy was reduced during IAV infection in

Ripk2$^{-/-}$ BMDCs by staining for LC3-II and mitochondria. The ratio of LC3-II puncta colocalized with mitochondria by confocal microscopy was significantly reduced in *Ripk2*$^{-/-}$ compared to WT BMDCs (Fig. 7g). These results indicate that the induction of mitophagy during IAV infection, which is regulated by NOD2 and RIPK2, is essential for the clearance of damaged mitochondria. In the absence of RIPK2 or NOD2, elevated mitochondrial SOX production enhances NLRP3 inflammasome activation.

RIPK2 regulates mitophagy through its kinase activity

It was previously reported that RIPK2 regulates autophagy through the autophagy protein ATG16L1[22, 23]. However, another group found no interaction between RIPK2 and ATG16L1[37]. To examine how RIPK2 regulates mitophagy during viral infection, we first examined the possibility that RIPK2 might interact with ATG16L1. We expressed RIPK2 and the autophagy related protein ATG16L1 in the presence or absence of NOD2 and IAV infection. IAV infection was required for association of RIPK2, NOD2 and ATG16L1 (Supplementary Fig. 8a). However, we were unable to coimmunoprecipitate endogenous RIPK2 and ATG16L1 or detect any significant colocalization by immunofluorescence confocal microscopy in BMDCs during IAV infection (data not shown). Although the overexpression data above suggests the interaction with ATG16L1 may play an important role during IAV infection, this remains to be verified under endogenous conditions. Furthermore, an interaction between RIPK2 and ATG16L1 still does not address the upstream signaling which initiates mitophagy during infection. To begin to address the exact mechanism by which mitophagy is regulated by RIPK2 in our model, we examined the role of RIPK2's kinase activity during mitophagy induction. Treatment of WT BMDCs with the p38 and RIPK2 inhibitor SB203580 resulted in reduced LC3-II conversion and increased caspase-1 activation as well as increased IL-18 production (Fig. 8a–b). We confirmed that this effect was due to RIPK2 inhibition by examining autophagy in p38$^{Flox/Flox}$ BMDCs. p38 deficiency did not impact LC3-II conversion during IAV infection, indicating the effect of SB203580 to be mediated by RIPK2 inhibition (Supplementary Fig. 8b). Next, we examined autophagy proteins known to be activated by phosphorylation and discovered that phosphorylation of ULK1 at Ser555 was reduced in *Ripk2*$^{-/-}$ BMDCs during IAV infection although upregulation of total ULK1 was not affected (Fig. 8c). Phosphorylation at Ser555 of ULK1 is known to be important for its activation and ULK1 is known to play an important role in mitophagy, especially during hematopoietic development[38]. We therefore examined *Ulk1*$^{-/-}$ BMDCs and found that they also have increased caspase-1 activation following IAV infection and this increased caspase-1 activation was suppressed by NAC treatment (Fig. 8d). Furthermore, *Ulk1*$^{-/-}$ BMDCs have more mitochondrial damage and increased mitochondrial mass compared to WT BMDCs (Fig. 8e–f and Supplementary Fig. 8c). Collectively, these data demonstrate that NOD2 and RIPK2 interact with each other in response to IAV vRNA genomes and regulate mitophagy in a RIPK2 kinase and ULK1 dependent manner. Mitophagy is then responsible for removing damaged mitochondria and preventing excessive NLRP3 activation and IL-18 production (Fig. 8g).

Discussion

Although the *in vivo* relevance of RIPK2-mediated signalling for immunity against bacterial pathogens has been clearly demonstrated for pathogens like *Helicobacter pylori* and *Listeria monocytogenes*[39, 40], the role of RIPK2 in the immune response to viral infections *in vivo* has not been reported. In addition, the involvement of RIPK2 in signaling pathways other than the regulation of NF-κB and MAP kinase has not been explored in detail.

The present analysis demonstrates that RIPK2 is critical for protection against IAV-induced immunopathology during IAV infection. Moreover, our results demonstrate that RIPK2 functions by negatively regulating IL-18 and IFN-γ production in stromal and immune cells of the pulmonary tract. In addition, we identify NOD2 as the NLR acting upstream of RIPK2 in mediating protection against IAV-induced morbidity and mortality. These results thus implicate NOD2 as a key partner in additional immune signaling pathways during viral infection, beyond those previously discovered for type I IFNs[25, 26].

Although we observed elevated IL-1β *in vitro* by infecting BMDCs with IAV, the amount of IL-1β present *in vivo* was on the order of 5–10 times lower than that of IL-18. These low amounts of IL-1β *in vivo* likely obscured our ability to detect differences in this cytokine initially. We expect that IL-1β may also play some role in our model *in vivo*; however, the importance of RIPK2-mediated dampening of IL-18 was illustrated by the marked effect of IL-18 neutralizing antibodies in reducing the morbidity and mortality in *Ripk2*-deficient mice infected with IAV and was further confirmed in *Ripk2*$^{-/-}$*Il18*$^{-/-}$ mice. This demonstrates that excessive IL-18 production in *Ripk2*$^{-/-}$mice drives the majority of the immunopathology.

Immunopathology is a key factor in acute fatal IAV pneumonia in humans and in animal models infected with highly virulent IAV strains[41, 42]. The present finding that IL-18 mediates hyper-inflammatory responses in *Ripk2*$^{-/-}$ mice thus opens new possibilities for the treatment of severe IAV infections. In other disease models, elevated IL-18 has been shown to promote neutrophil infiltration, and to mediate the production of IFN-γ and chemokines (LPS toxemia and ischemic reperfusion, respectively). Reducing IL-18 in these experimental systems limits the extent of tissue damage and promotes survival[43, 44]. Blocking IL-18 may limit the extent of lung immunopathology in situations where IAV infection leads to extreme respiratory distress.

At the molecular level, our data show that RIPK2 dampens harmful IL-18-driven inflammatory responses against IAV by preventing excessive activation of caspase-1 through a mitophagy-mediated suppression mechanism, rather than via a direct interaction with caspase-1. Multiple inflammasomes that activate caspase-1 in a pathogen-dependent manner have been identified. However, our previous studies identified a critical role for the NLRP3 inflammasome in regulating IL-1β and IL-18 production to IAV infection both *in vivo* and *in vitro*[12, 13]. We here extended these findings by showing that RIPK2-mediated inhibition of inflammasome activation proceeds through the removal of damaged mitochondria and reduction of mitochondrial SOX production, a known activator of the

NLRP3 inflammasome[35, 45]. The role for the NLRP3 inflammasome in our model was also verified by treatment with the NLRP3 specific inhibitor glyburide.

Many reports differ on the mechanism by which RIPK2 regulates the induction of autophagy or xenophagy in response to bacterial infection[20, 22, 23, 37]. In fact there are differing reports on the role of RIPK2 and ATG16L1 during bacterial infection[22, 23, 37]. Although we observed an interaction between these two proteins when overexpressed, we were unable to verify this interaction in BMDCs during IAV infection, despite the use of multiple methods and conditions. We therefore sought out other potential mechanisms by which RIPK2 could regulate autophagy. We discovered that *Ripk2*$^{-/-}$ BMDCs had increased mitochondrial damage and more mitochondrial mass, suggesting that mitophagy was defective. In our search to identify the mechanisms involved in RIPK2 mediated mitophagy, we examined the mitophagy protein Parkin through the use of Parkin deficient mice (*Park2*$^{-/-}$). However, we were unable to observe any role for Parkin in our model (data not shown). In the end, we discovered that activation of ULK1 by phosphorylation at Ser555 was reduced in *Ripk2*$^{-/-}$ BMDCs. The importance of ULK1 was also verified in our model as *Ulk1*$^{-/-}$ BMDCs phenocopy *Ripk2*$^{-/-}$ BMDCs with regard to mitochondrial damage and inflammasome activation. Our findings highlight a signaling pathway in which NOD2 and RIPK2 respond to viral infection by promoting ULK1 phosphorylation and inducing mitophagic responses which dampen inflammasome activation and IL-18 production. Although it is clear that Ripk2 deficiency results in reduced ULK1 phosphorylation, it is not clear whether RIPK2 directly phosphorylates ULK1 or if there are other intermediates which are regulated by RIPK2 which subsequently activate ULK1.

It should be noted that autophagy was recently shown to directly clear inflammasomes from activated cells, thus modulating inflammation[17]. However, we were unable to observe any role for autophagy in our system during *Listeria* infection dependent upon the AIM2 inflammasome, suggesting that global inflammasome degradation by macroautophagy is likely not important in our model. Furthermore, virus replication was not affected in our model, suggesting that xenophagy also does not play a significant role. Therefore, our data are the first to demonstrate that NOD2-RIPK2 signaling can regulate mitophagy specifically during viral infection and to demonstrate the physiological relevance of this pathway in controlling pulmonary inflammation *in vivo*. It should also be noted that *Rikp2*$^{-/-}$ cells had slightly higher basal levels of mitochondrial mass and damaged mitochondria. These data may indicate a role for Ripk2 in the steady state regulation of mitophagy. In the future it will be of interest to examine whether this can exacerbate other non-infectious diseases where mitochondrial damage or metabolic stresses are known to be factors. In all, our findings demonstrate that NOD2-RIPK2 signaling is involved in the recognition of a wider variety of pathogens than previously thought, and we determined that RIPK2 can regulate ULK1 mediated mitophagy. Finally, our results provide a unifying principle by linking NOD2-RIPK2 signaling, autophagy or mitophagy, and inflammasome-IL-18 production together, suggesting that this pathway is a critical regulatory mechanism for preventing overt inflammation under certain disease conditions.

Materials and Methods

Virus, bacteria and ligands

The influenza A/Puerto Rico/8/34 H1N1 virus (PR8) was generated by an eight-plasmid reverse genetics system[46]. X31 virus was prepared similarly. Stocks were propagated no more than twice by allantoic inoculation of 10-day-old embryonated hen's eggs with seed virus diluted 1:10^4. *Listeria monocytogenes* was grown in brain heart infusion medium at 37 °C overnight and then subcultured to mid-log phase for infections. Poly I:C and Poly I:C lyovec were obtained from Invivogen and used at the indicated concentrations. IAV genomes, or cellular mRNA controls, were purified from viral stocks or BMDCs using Trizol LS and transfected using Lipofectamine 2000 according to manufactures instructions.

Measuring virus titers

Near confluent 9.6 cm^2 monolayers of Madin-Darby Canine Kidney (MDCK) cells were infected with 1 mL aliquots of 6×10-fold dilutions of lung homogenate, washed and overlayed with 3 ml minimum essential medium (MEM) containing 1 mg/ml L-1-tosylamido-2-phenylethyl chloromethyl ketone-treated trypsin (Sigma Aldrich) and 1.0% Sea Plaque agarose (Lonza). After 3 days, plaques were visualized with crystal violet.

Mice

All mice were maintained at SJCRH and were fully on the C57BL/6J (B6) background. *Nod2*$^{-/-}$, LysM-Cre^{+} Atg7$^{flox/flox}$ GFP-LC3^{+}, p38$^{flox/flox}$ (Mapk14$^{flox/flox}$ Rosa26-Cre-ER^{T2}), *Ulk1*$^{-/-}$ and *Ripk2*$^{-/-}$ [24, 32, 40, 47–49] mice have been reported previously and *Ripk2*$^{-/-}$ × *IL-18*$^{-/-}$ double deficient mice were generated by backcrossing. All mice were housed in a specific pathogen free (SPF) facility and experiments were conducted under protocols approved by the St. Jude Children's Research Hospital Committee on Use and Care of Animals.

Virus infection and sampling

Mice were anaesthetized with Avertin (2,2,2-tribromoethanol) and infected i.n. with the indicated dose of the PR8 virus in 30μL of endotoxin-free PBS. In the case of IL-18 neutralization, mice were injected as indicated with 200μL of rabbit antiserum against mouse IL-18 (C. A. Dinarello). For *in vivo* autophagy induction, mice were injected with 600μg/kg of rapamycin on D0, 1 and 2 and samples were collected 6h after the final injection. Mice were either weighed and monitored for severe illness daily for a period of 14–16d, or taken at various intervals for sampling the whole lung. The right lungs were processed by mincing and passing through a 70μm cell strainer using a total of 4ml HBSS. Following light centrifugation, total cell numbers per lung or lymph node were determined and stained for flow cytometry. In addition, HBSS supernatant was used for virus titration and cytokine analysis. The left lungs were used for histopathological analysis or ground in RIPA buffer + protease inhibitor + phosphatase inhibitor (Calbiochem) followed by boiling in sodium dodecyl sulfate (SDS) sample buffer and examination by Western blot.

Flow cytometry

Aliquots of whole lung populations (as above) were stained for myeloid cells with anti-CD11b, anti-MHC Class II, anti-GR1, anti-CD11c (Biolegend, M1/70, M5/114.15.2, RB6-8C5, N418) MAbs, and annexin V after blocking the Fc receptor with anti-CD32/CD16 MAb (from BD Pharmingen) at 4°C, and analyzed by flow cytometry. (macrophages=$CD11b^{+}$,$CD11c^{-}$,$GR1^{-,lo}$; granulocytes=$CD11b^{hi}$,$CD11c^{-}$,$GR1^{hi}$; DCs=$CD11c^{+}$, MHC Class II^{+}) Additionally, lymphocytes were stained with anti-CD19, anti-TCRβ, anti-CD8, and anti-CD4 (Biolegend, 6D5, H57–597, 53–6.7, RM4–5). NK and NKT cells were stained with anti-CD3 and anti-NK1.1 (Biolegend, 145-2C11, PK136). For NK, NKT and $CD8^{+}$ T cell activation experiments, anti-CD3 and anti-NK1.1 or anti-TCRβ, anti-CD8 and anti-CD44 (Biolegend, IM7) markers were used. Intracellular IFN-γ (Biolegned, XMG1.2) in $CD8^{+}$ T cells was measured after stimulation of whole lung cells for 5h at 37°C and 5% CO_2 with a cocktail of IAV peptides (PB1, PB1-F2, NP, PA, M1) at 1ug/ml each with monensin. NK and NKT cells were similarly restimulated with 10ng/ml IL-12. Cell numbers are 1/10 of the total number present in the right lung lobes or 1/3 of the number present in the mediastinal lymph node

For staining mitochondria, BMDCs were uninfected as controls or infected for 6h with *Listeria* or 18–24h with PR8 influenza and then stained for 30 min in fresh complete RPMI1640 medium containing 5μM MitoSOX or 2μM MitoTracker Green. Cells were then washed in HBSS, resuspended in FACS buffer and analyzed immediately by flow cytometry.

Assaying for cytokines and chemokines

Mouse cytokines and chemokines in HBSS supernatants from whole lung homogenates were measured using the Millipore 22-multiplex assay following the manufacturer's instructions. In addition, lung samples and supernatants from BMDC cultured *in vitro* were assayed by ELISA for IL-18 (MBL International, Woburn, MA) and IL-1β or IFN-γ (eBiosciences). All cytokines from lung homogenates were normalized to the total protein in the homogenate by BCA protein assay (Pierce) and expressed as cytokine concentration per milligram total protein (pg/mg t.p.)

Histopathological analysis, transmission electron microscopy and confocal microscopy

Formalin-preserved left lungs were embedded in paraffin and processed by standard techniques. Longitudinal 5μm sections were stained with H&E and examined by an experienced pathologist blinded to the experimental groups. For immunohistochemistry, formalin-fixed paraffin-embedded tissues were cut into 4-μm sections and slides were stained with Abs to identify IL-18 (MBL International, Woburn, MA, clone 39–3F) and neutrophils (7/4 monoclonal antibody, Invitrogen).

For transmission electron microscopy, cells were fixed in a solution of 2.0% paraformaldahyde + 2.5% glutaraldehyde in 0.1 m cacodylate buffer (pH 7.4). Cells were then embedded and sectioned for transmission electron microscopy by the Cell and Tissue Imaging Core Facility of St. Jude Children's Research Hospital.

For examination of $LC3^+$ puncta numbers or colocalization with mitochondria by confocal microscopy, BMDCs were infected with IAV at 10MOI and/or treated with 50μM chloroquine (Calbiochem) 1h after infection. After 18h, cells were treated with 100nM MitoTracker Orange CMTMRos for 30min. Cells were then fixed in 4% paraformaldehyde in PBS+100mM HEPES buffer. Cells were permeablized with methanol at −20°C for 5 min, washed 3× in PBS, and then blocked using 1× assay buffer (eBiosciences) + 0.1%Triton ×100 for 1h. Cells were stained overnight at 4°C with a 1:500 dilution of anti-LC3B antibody (Novus Biologicals, NB600–1384) in blocking buffer. Cells were washed 3× and then stained with Alexa488 donkey anti-rabbit secondary (Invitrogen, A-21206) for 2h in blocking buffer. Cells were washed an additional 3× and then mounted using Prolong GOLD with DAPI (Invitrogen) and examined on a Nikon C1Si laser scanning confocal microscope. Data analysis was performed using ImageJ.

Generation of bone marrow chimeras

WT (CD45.1) and *Ripk2*$^{-/-}$ (CD45.2) mice, were lethally irradiated with a split dose of 1200 rads (800,400), then injected with 5×10^6 bone marrow (BM) cells from the indicated donors. Mice were allowed to recover for 6 weeks to ensure successful engraftment. The extent of BM reconstitution was verified by staining lymphocytes with anti-CD45.1 APC and anti-CD45.2 FITC (Biolegend, A20, 104) for congenic markers, and was always > 90%.

Cell signaling, caspase-1 activation and IL-18 production *in vitro*

WT, *Nod2*$^{-/-}$ and *Ripk2*$^{-/-}$ bone marrow derived dendritic cells (BMDC) were differentiated in complete RPMI containing 10% heat-inactivated FBS and supplemented with 20ng/ml murine GM-CSF at 37°C in a humidified atmosphere containing 5% CO_2 for 7 days. Cells were mock infected, or infected with 10 MOI PR8 or 10 MOI ×31 for 24h or 10 MOI *Listeria monocytogenes* for 4–6h in antibiotic free medium. For N-acetyl cysteine (NAC, Sigma-Aldrich) or mitoTEMPO (Enzo Life Sciences) treatment, BMDCs were infected with 10 MOI PR8 for 1h and then fresh RPMI 1640 with 10% FBS containing the indicated concentrations of inhibitors were added. Other inhibitors, including glyburide (Sigma-Aldrich), rapamycin or SB203580 (Calbiochem) were also added 1h after infection. 18–24h later, supernatants were collected for ELISA and cells were lysed with RIPA buffer + protease inhibitor + phosphatase inhibitor (Calbiochem), followed by boiling in sodium dodecyl sulfate (SDS) sample buffer and examination by Western blot. Anti-caspase-1 (Adipogen, AG-20B-0042), anti-ULK1 (Sigma-Aldrich, A7481), anti-LC3 (Novus Biologicals, NB600–1384), and anti-pUlk1 Ser555 (Cell Signaling Technologies, D1H4), were used for Western blot detection and equal loading was verified by blotting with anti-GAPDH or anti-β-Tubulin (Cell signaling Technologies, D16H11, 9F3). HRP-labeled anti-rabbit antibodies were obtained from Jackson Immuno Research.

Overexpression and Coimmunoprecipitation

293T cells were transfected using Lipofectamine 2000 (Invitrogen) or Xfect (Clontech) according to the manufacturer's protocol and harvested 24h after transfection for examination by coimmunoprecipitation (CoIP) and/or by Western blot. For CoIP, 3–4 10cm wells each were transfected with pCMV6-Kan/Neo-RIPK2 (Origene), pBK-flag-NOD2, or

pCMV-3xMyc-ATG16L1 and cells were lysed after 24h in DPBS with 1% NP40 + protease inhibitors + phosphatase inhibitors (Calbiochem). In some experiments, 293T cells were also infected with 10 MOI influenza A/PR/8/34 H1N1 1h prior to transfection. CoIP was performed overnight at 4°C with protein A/G PLUS agarose beads (SantaCruz) and rabbit anti-RIPK2 (SantaCruz, H300), mouse anti-Flag (Sigma, M2), and rabbit anti-Myc (SantaCruz, A14) antibodies. Western blot was then performed with rabbit anti-RIPK2, rabbit anti-Flag (Sigma, F7425), rabbit anti-Myc and Exactacruz HRP anti-rabbit secondary (SantaCruz, SC-45043).

Statistical analysis

Data are represented as mean ± SEM. Statistical significance was determined by a Student *t*-test, one-way ANOVA for multiple comparisons, and Kaplan-Meier Survival Plot and LogRank Test for survival data. Data for $LC3^+$ puncta was not normally distributed and data were analyzed by the Mann Whitney test. P values ≤0.05 were considered statistically significant.

Supplementary Material

Refer to Web version on PubMed Central for supplementary material.

Acknowledgements

We thank the veterinary pathology core lab (VPCL) at St. Jude for their work in processing of H&E and IHC slides. We also thank the Cell and Tissue Imaging Core Facility for their help in preparing and imaging TEM samples. We thank Anthony Coyle, Ethan Grant, John Bertin (Millennium Pharmaceuticals), Tak Mak (University of Toronto) and Richard Flavell (Yale University) for generous supply of mutant mice. ML is supported by grants from the European Union Framework Program 7 (Marie-Curie Grant 256432), European Research Council (grant 281600) and the Fund for Scientific Research Flanders (G030212N, 1.2.201.10.N.00 and 1.5.122.11.N.00). This work was supported by National Institute of Health Grants (AR056296, AI101935 and CA163507), and the American Lebanese Syrian Associated Charities (ALSAC) to T.-D.K.

References

1. Kilbourne ED. Influenza pandemics of the 20th century. Emerg Infect Dis. 2006; 12:9–14. [PubMed: 16494710]
2. Taubenberger JK, Morens DM. 1918 Influenza: the mother of all pandemics. Emerg Infect Dis. 2006; 12:15–22. [PubMed: 16494711]
3. de Jong MD, et al. Fatal outcome of human influenza A (H5N1) is associated with high viral load and hypercytokinemia. Nat Med. 2006; 12:1203–1207. [PubMed: 16964257]
4. Kobasa D, et al. Aberrant innate immune response in lethal infection of macaques with the 1918 influenza virus. Nature. 2007; 445:319–323. [PubMed: 17230189]
5. Perrone LA, Plowden JK, Garcia-Sastre A, Katz JM, Tumpey TM. H5N1 and 1918 pandemic influenza virus infection results in early and excessive infiltration of macrophages and neutrophils in the lungs of mice. PLoS Pathog. 2008; 4:e1000115. [PubMed: 18670648]
6. Tumpey TM, et al. Characterization of the reconstructed 1918 Spanish influenza pandemic virus. Science. 2005; 310:77–80. [PubMed: 16210530]
7. Guillot L, et al. Involvement of toll-like receptor 3 in the immune response of lung epithelial cells to double-stranded RNA and influenza A virus. J Biol Chem. 2005; 280:5571–5580. [PubMed: 15579900]
8. Heer AK, et al. TLR signaling fine-tunes anti-influenza B cell responses without regulating effector T cell responses. J Immunol. 2007; 178:2182–2191. [PubMed: 17277123]

9. Rehwinkel J, et al. RIG-I detects viral genomic RNA during negative-strand RNA virus infection. Cell. 140:397–408. [PubMed: 20144762]
10. Allen IC, et al. The NLRP3 inflammasome mediates in vivo innate immunity to influenza A virus through recognition of viral RNA. Immunity. 2009; 30:556–565. [PubMed: 19362020]
11. Ichinohe T, Pang IK, Iwasaki A. Influenza virus activates inflammasomes via its intracellular M2 ion channel. Nat Immunol. 11:404–410. [PubMed: 20383149]
12. Thomas PG, et al. The intracellular sensor NLRP3 mediates key innate and healing responses to influenza A virus via the regulation of caspase-1. Immunity. 2009; 30:566–575. [PubMed: 19362023]
13. Kanneganti TD, et al. Critical role for Cryopyrin/Nalp3 in activation of caspase-1 in response to viral infection and double-stranded RNA. J Biol Chem. 2006; 281:36560–36568. [PubMed: 17008311]
14. Martinon F, Burns K, Tschopp J. The inflammasome: a molecular platform triggering activation of inflammatory caspases and processing of proIL-beta. Mol Cell. 2002; 10:417–426. [PubMed: 12191486]
15. Schroder K, Tschopp J. The inflammasomes. Cell. 140:821–832. [PubMed: 20303873]
16. Mortimore GE, Hutson NJ, Surmacz CA. Quantitative correlation between proteolysis and macro- and microautophagy in mouse hepatocytes during starvation and refeeding. Proc Natl Acad Sci U S A. 1983; 80:2179–2183. [PubMed: 6340116]
17. Shi CS, et al. Activation of autophagy by inflammatory signals limits IL-1beta production by targeting ubiquitinated inflammasomes for destruction. Nat Immunol. 13:255–263. [PubMed: 22286270]
18. Geisler S, et al. The PINK1/Parkin-mediated mitophagy is compromised by PD-associated mutations. Autophagy. 2010; 6:871–878. [PubMed: 20798600]
19. Sandoval H, et al. Essential role for Nix in autophagic maturation of erythroid cells. Nature. 2008; 454:232–235. [PubMed: 18454133]
20. Anand PK, et al. TLR2 and RIP2 pathways mediate autophagy of Listeria monocytogenes via extracellular signal-regulated kinase (ERK) activation. J Biol Chem. 286:42981–42991. [PubMed: 22033934]
21. Uhl M, et al. Autophagy within the antigen donor cell facilitates efficient antigen crosspriming of virus-specific CD8+ T cells. Cell death and differentiation. 2009; 16:991–1005. [PubMed: 19229247]
22. Cooney R, et al. NOD2 stimulation induces autophagy in dendritic cells influencing bacterial handling and antigen presentation. Nat Med. 16:90–97. [PubMed: 19966812]
23. Homer CR, Richmond AL, Rebert NA, Achkar JP, McDonald C. ATG16L1 and NOD2 interact in an autophagy-dependent antibacterial pathway implicated in Crohn's disease pathogenesis. Gastroenterology. 139:1630–1641. 1641, e1631–1632. [PubMed: 20637199]
24. Kobayashi K, et al. RICK/Rip2/CARDIAK mediates signalling for receptors of the innate and adaptive immune systems. Nature. 2002; 416:194–199. [PubMed: 11894098]
25. Dugan JW, et al. Nucleotide oligomerization domain-2 interacts with 2′–5′-oligoadenylate synthetase type 2 and enhances RNase-L function in THP-1 cells. Mol Immunol. 2009; 47:560–566. [PubMed: 19853919]
26. Sabbah A, et al. Activation of innate immune antiviral responses by Nod2. Nat Immunol. 2009; 10:1073–1080. [PubMed: 19701189]
27. Park JH, et al. RICK/RIP2 mediates innate immune responses induced through Nod1 and Nod2 but not TLRs. J Immunol. 2007; 178:2380–2386. [PubMed: 17277144]
28. Ishikawa H, et al. IFN-gamma production downstream of NKT cell activation in mice infected with influenza virus enhances the cytolytic activities of both NK cells and viral antigen-specific CD8+ T cells. Virology. 407:325–332. [PubMed: 20855097]
29. Okamura H, et al. Cloning of a new cytokine that induces IFN-gamma production by T cells. Nature. 1995; 378:88–91. [PubMed: 7477296]
30. Kim S, et al. Listeria monocytogenes is sensed by the NLRP3 and AIM2 inflammasome. Eur J Immunol. 2010; 40:1545–1551. [PubMed: 20333626]

31. Black RA, Kronheim SR, Merriam JE, March CJ, Hopp TP. A pre-aspartate-specific protease from human leukocytes that cleaves pro-interleukin-1 beta. J Biol Chem. 1989; 264:5323–5326. [PubMed: 2784432]
32. Lamkanfi M, et al. Glyburide inhibits the Cryopyrin/Nalp3 inflammasome. The Journal of cell biology. 2009; 187:61–70. [PubMed: 19805629]
33. Tsuchiya K, et al. Involvement of absent in melanoma 2 in inflammasome activation in macrophages infected with Listeria monocytogenes. J Immunol. 2010; 185:1186–1195. [PubMed: 20566831]
34. Sarkar A, et al. ASC directs NF-kappaB activation by regulating receptor interacting protein-2 (RIP2) caspase-1 interactions. J Immunol. 2006; 176:4979–4986. [PubMed: 16585594]
35. Nakahira K, et al. Autophagy proteins regulate innate immune responses by inhibiting the release of mitochondrial DNA mediated by the NALP3 inflammasome. Nat Immunol. 12:222–230. [PubMed: 21151103]
36. Saitoh T, et al. Loss of the autophagy protein Atg16L1 enhances endotoxin-induced IL-1beta production. Nature. 2008; 456:264–268. [PubMed: 18849965]
37. Travassos LH, et al. Nod1 and Nod2 direct autophagy by recruiting ATG16L1 to the plasma membrane at the site of bacterial entry. Nat Immunol. 11:55–62. [PubMed: 19898471]
38. Joo JH, et al. Hsp90-Cdc37 chaperone complex regulates Ulk1- and Atg13-mediated mitophagy. Molecular cell. 2011; 43:572–585. [PubMed: 21855797]
39. Viala J, et al. Nod1 responds to peptidoglycan delivered by the Helicobacter pylori cag pathogenicity island. Nat Immunol. 2004; 5:1166–1174. [PubMed: 15489856]
40. Kobayashi KS, et al. Nod2-dependent regulation of innate and adaptive immunity in the intestinal tract. Science. 2005; 307:731–734. [PubMed: 15692051]
41. Kash JC, et al. Genomic analysis of increased host immune and cell death responses induced by 1918 influenza virus. Nature. 2006; 443:578–581. [PubMed: 17006449]
42. Rainsford KD. Influenza (“Bird Flu”), inflammation and anti-inflammatory/analgesic drugs. Inflammopharmacology. 2006; 14:2–9. [PubMed: 16835706]
43. Netea MG, et al. Neutralization of IL-18 reduces neutrophil tissue accumulation and protects mice against lethal Escherichia coli and Salmonella typhimurium endotoxemia. J Immunol. 2000; 164:2644–2649. [PubMed: 10679104]
44. Raeburn CD, et al. Neutralization of IL-18 attenuates lipopolysaccharide-induced myocardial dysfunction. Am J Physiol Heart Circ Physiol. 2002; 283:H650–657. [PubMed: 12124212]
45. Zhou R, Yazdi AS, Menu P, Tschopp J. A role for mitochondria in NLRP3 inflammasome activation. Nature. 469:221–225. [PubMed: 21124315]
46. Hoffmann E, Krauss S, Perez D, Webby R, Webster RG. Eight-plasmid system for rapid generation of influenza virus vaccines. Vaccine. 2002; 20:3165–3170. [PubMed: 12163268]
47. Takeda K, et al. Defective NK cell activity and Th1 response in IL-18-deficient mice. Immunity. 1998; 8:383–390. [PubMed: 9529155]
48. Huang G, et al. Signaling via the kinase p38alpha programs dendritic cells to drive TH17 differentiation and autoimmune inflammation. Nat Immunol. 2012; 13:152–161. [PubMed: 22231518]
49. Kundu M, et al. Ulk1 plays a critical role in the autophagic clearance of mitochondria and ribosomes during reticulocyte maturation. Blood. 2008; 112:1493–1502. [PubMed: 18539900]

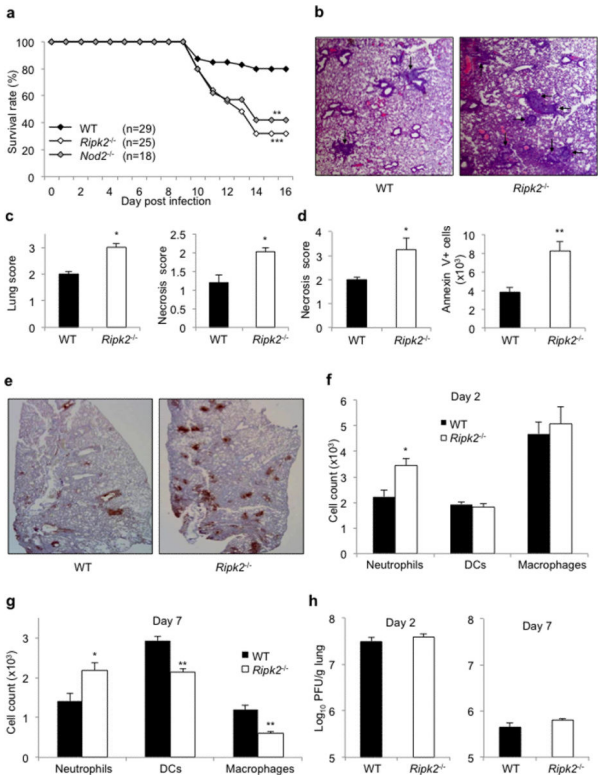

Figure 1. RIPK2 deficiency leads to hyper-inflammation

(**a**) Mice were infected intra-nasally (i.n.) with 750 PFU of the PR8 virus and examined daily for survival and clinical features of disease. (**b**) H&E-stained lung sections from mice infected with PR8 virus on day 2. Cellular infiltrates and necrotic debris occluding the airways are indicated with arrows. (**c**) H&E-stained lung sections were prepared on day 2 post-infection and scored for disease severity and necrosis. (**d**) The extent of cell death on day 7 was estimated visually on H&E-stained lung sections (necrosis score), and by flow cytometry for annexin V-stained lung cell populations. (**e**) Immunohistochemistry (IHC) staining of neutrophils occluding the airways of PR8 infected *Ripk2*$^{-/-}$ mice. (**f-g**) Flow cytometric analysis of neutrophil, DC and macrophage cell numbers on days 2 and 7. (**h**) Pulmonary viral titers on days 2 and 7 after infection in *Ripk2*$^{-/-}$ and WT mice. a,f,g,h: Data are cumulative from 3 independent experiments (g-h: n=10–12). b-e: Data are representative of 2-3 independent experiments n=3–7 per group/experiment (mean +/−SEM, *p<0.05, **p<0.01, ***p<0.001).

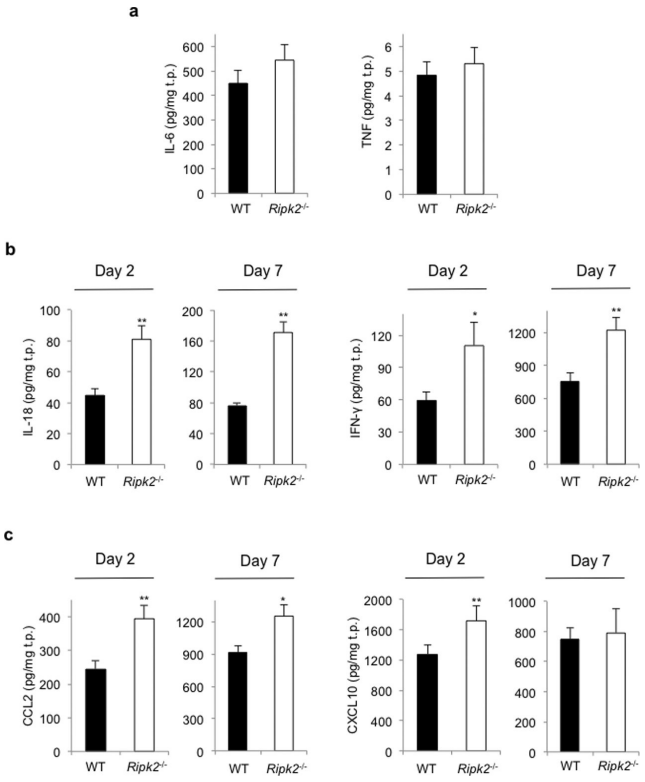

Figure 2. RIPK2 modulates cytokine and chemokine production

Supernatants of whole lung homogenates taken on d2 and d7 after infection with the PR8 virus were analyzed for IL-6 and TNF (**a**), IL-18 and IFN-γ (**b**), and a set of chemokines (**c**). Data were normalized for total protein from lung homogenates (pg/mg total protein (t.p.)). Data are cumulative from 3 independent experiments, n=10–12 mice. (mean +/−SEM, *p<0.05, **p<0.01).

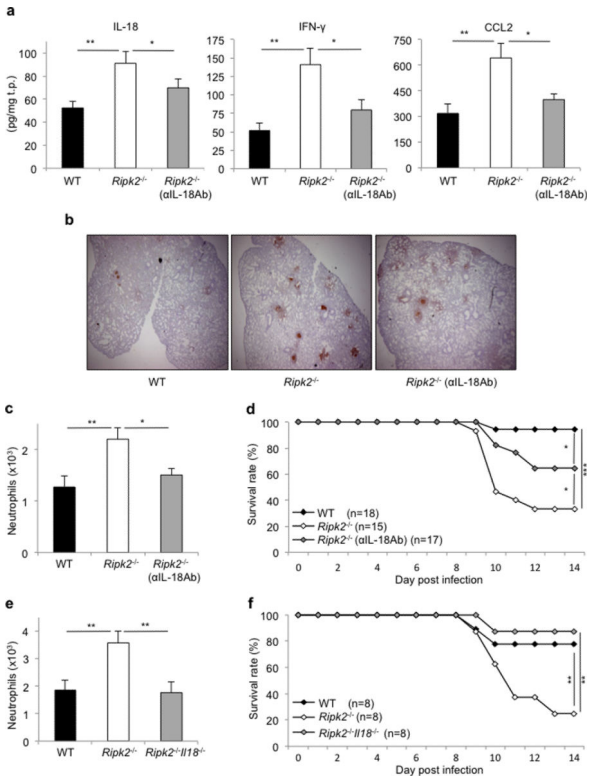

Figure 3. IL-18 mediates hyper-inflammation in *Ripk2*$^{-/-}$ mice

Ripk2$^{-/-}$ mice were injected i.p. with anti-IL-18 neutralizing antiserum (αIL-18Ab) 3h prior to infection with the PR8 virus. Mice were examined on d2 for IL-18, IFN-γ, and CCL2 levels in whole lung homogenates (**a**), and for neutrophil numbers by IHC (**b**) and by flow cytometry (**c**). (**d**) Analysis of survival of infected *Ripk2*$^{-/-}$ mice that were treated with IL-18 neutralizing antibodies. (**e**) IL-18 was deleted from *Ripk2*$^{-/-}$ mice (*Ripk2*$^{-/-}$*Il18*$^{-/-}$mice) and neutrophilia examined on d2 following PR8 infection. (**f**) Survival of *Ripk2*$^{-/-}$*Il18*$^{-/-}$ mice compared to *Ripk2*$^{-/-}$ or WT mice. Data are representative of 2 independent experiments, n=6–8 per group/experiment. (mean +/−SEM, *p<0.05, **p<0.01, ***p<0.001). (t.p.=total protein)

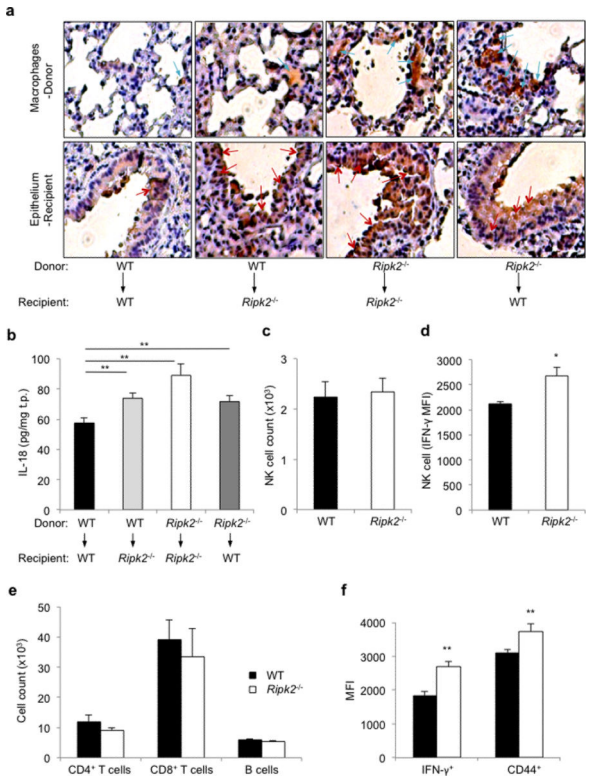

Figure 4. Both hematopoietic and lung epithelial cells contribute to hypercytokinemia

RIPK2 bone marrow chimeras were analyzed at d2 after PR8 infection for contribution to elevated IL-18 production by using (**a**) IL-18 IHC and (**b**) IL-18 ELISA of whole lung homogenates. (**c**) Flow cytometric analysis of NK cell counts in *Ripk2*$^{-/-}$ and WT mice. (**d**) Analysis of WT and *Ripk2*$^{-/-}$ NK cells for IFN-γ production on a per cell basis. (**e**) Accumulation of T and B cells in lungs. (**f**) Analysis of CD8^{+} T cells for IFN-γ and CD44 expression in WT and *Ripk2*$^{-/-}$ mice. Data are representative of 2–3 independent experiments, n=6–8 per group/experiment. (mean +/−SEM, *p<0.05, **p<0.01). For (**a**), blue arrows denote IL-18^{+} macrophages, and red arrows denote IL-18^{+} bronchial epithelium.

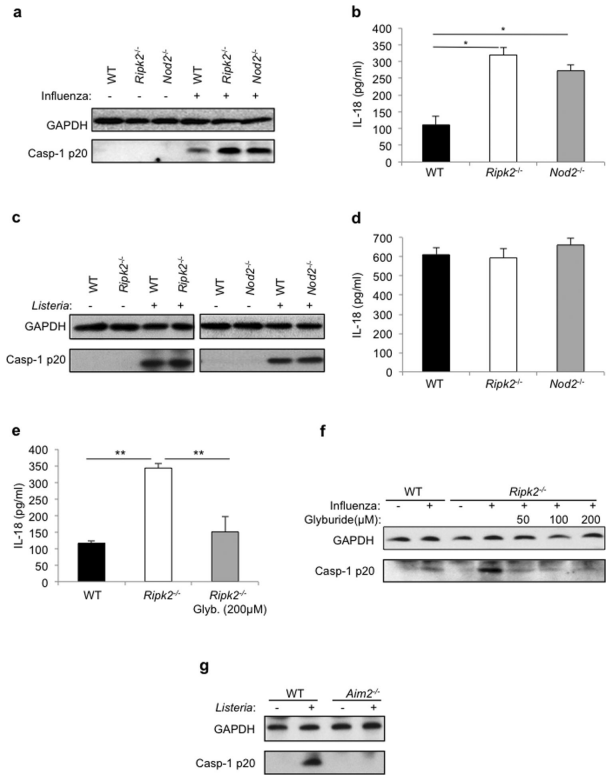

Figure 5. Elevated IL-18 in *Ripk2*$^{-/-}$ cells is NLRP3 inflammasome dependent

(**a**) Increased activation of caspase-1 (casp-1) in *Ripk2*$^{-/-}$ and *Nod2*$^{-/-}$ BMDCs following PR8 infection was analyzed by probing for active casp-1 p20 in immunoblots compared to GAPDH loading controls. (**b**) IL-18 release in PR8-infected *Ripk2*$^{-/-}$ and *Nod2*$^{-/-}$ BMDCs. (**c, d**) BMDCs infected with 10 MOI *Listeria monocytogenes* for 4h were analyzed for casp-1 activation by immunoblot and IL-18 production. (**e, f**) IL-18 and casp-1 activation in *Ripk2*$^{-/-}$ BMDCs treated with the NLRP3 inflammasome specific inhibitor glyburide during PR8 infection. (**g**) Immunoblot for casp-1 p20 during *Listeria* infection of WT and *Aim2*$^{-/-}$ BMDCs. Data are representative of 3–6 independent experiments with n=3 per experiment. (mean +/−SEM; *p<0.01, **p<0.001).

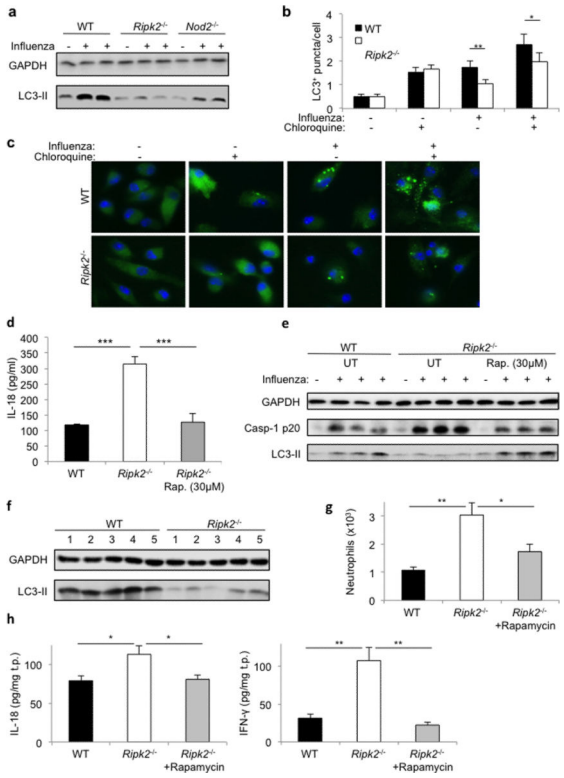

Figure 6. RIPK2 modulates inflammasome activation through autophagy

(**a**) *Ripk2*$^{-/-}$ and *Nod2*$^{-/-}$ BMDCs were analyzed by LC3-II imunoblotting as a marker for autophagy after 18h PR8 infection. (**b, c**) LC3-II^{+} puncta were counted in at least 100 cells from 5 random fields from confocal images of BMDCs following PR8 infection and/or chloroquine treatment. (**d, e**) Immunoblots of LC3-II and casp-1 and IL-18 production were determined in WT and *Ripk2*$^{-/-}$BMDCs following treatment with rapamycin (Rap). (**f**) LC3-II levels in the lungs of PR8 infected WT and *Ripk2*$^{-/-}$ mice. (**g, h**) Lung neutrophil infiltration, IL-18 and IFN-γ levels in IAV infected *Ripk2*$^{-/-}$ mice treated with rapamycin. (a–e) Data are representative of 2–6 independent experiments with n=2–3 per experiment. (f–h) Data are representative of 2 independent experiments for a total n=10–14 (mean +/−SEM; *p<0.05, **p<0.01, ***p<0.001).

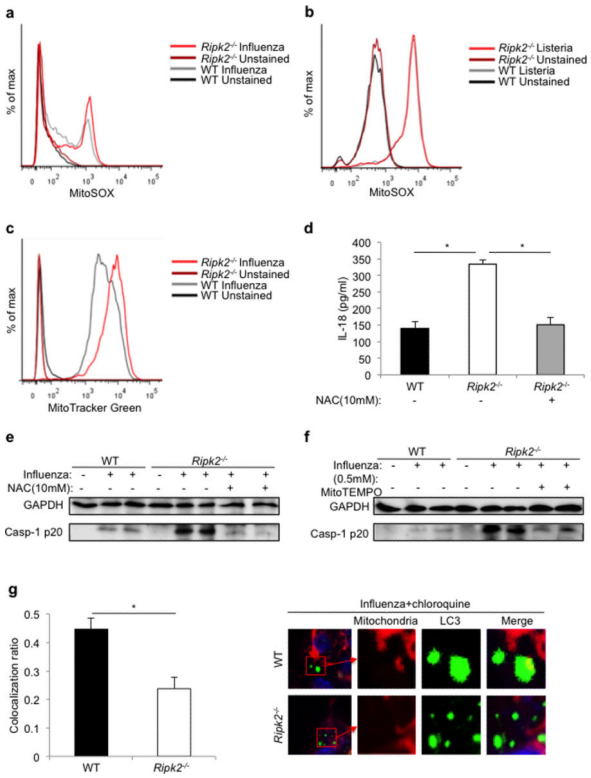

Figure 7. RIPK2 specifically regulates mitophagy and accumulation of damaged mitochondria to modulate inflammasome activation

(**a, b**) Staining of BMDCs with the mitochondrial superoxide (SOX) specific stain MitoSOX during IAV or *Listeria* infection. (**c**) Staining of WT and *Ripk2*$^{-/-}$ BMDCs with the general mitochondrial stain MitoTracker Green during IAV infection. (**d, e**) Analysis of IL-18 production and casp-1 activation in IAV-infected BMDCs that were pre-treated with the ROS inhibitor N-acetyl cysteine (NAC). (**f**) Analysis of casp-1 p20 in cell lysates of IAV-infected BMDCs pre-treated with the mitochondrial SOX inhibitor mitoTEMPO. (**g**) Confocal microscopy was used to analyze BMDCs stained for mitochondria (red) and LC3-II (green) for colocalization as an indicator of mitophagy. (a–f) Data are representative of 3–9 independent experiments with n=2–3 per experiment. (g) Data are representative of 2 independent experiments (mean +/−SEM; *p<0.01).

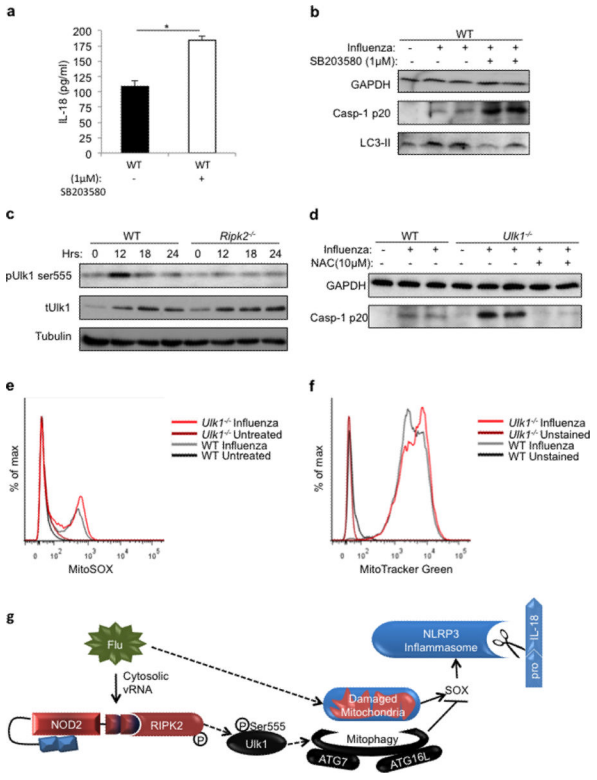

Figure 8. RIPK2 regulates activation of the critical autophagy protein ULK1 in response to IAV infection

(**a, b**) Casp-1 p20 and LC3-II immunoblots and IL-18 levels in PR8-infected WT BMDCs treated with the p38 and RIPK2 kinase inhibitor SB203580. (**c**) Immunoblots of phosphorylation of ULK1 at Ser555 in WT and *Ripk2*$^{-/-}$ BMDCs following PR8 infection. (**d**) Casp-1 activation in untreated or NAC treated WT and *Ulk1*$^{-/-}$ BMDCs following PR8 infection. (**e**) MitoSOX staining by flow cytometry in PR8-infected *Ulk1*$^{-/-}$ BMDCs. (**f**) MitoTracker Green staining of PR8-infected *Ulk1*$^{-/-}$ BMDCs. (**g**) Schematic diagram of the NOD2/RIPK2 dependent mechanism for mitophagy and subsequent NLRP3 inflammasome regulation. (a–f) Data are representative of 2–3 independent experiments with total n=4–6. (mean +/−SEM; *p<0.05).